Available online at www.sciencedirect.com
SCIENCE DIRECT
Journal of Catalysis 238 (2006) 458–467
JOURNAL OF CATALYSIS
www.elsevier.com/locate/jcat

Effect of alumina and titania on the oxidation of CO over Au nanoparticles evaluated by ^{13}C isotopic transient analysis

Jason T. Calla [a], Mangesh T. Bore [b], Abhaya K. Datye [b], Robert J. Davis [a,*]

[a] *Department of Chemical Engineering, University of Virginia, Charlottesville, VA 22094-4741, USA*
[b] *Department of Chemical and Nuclear Engineering and Ceramic and Composite Materials Center, University of New Mexico, MSC 01 1120, Albuquerque, NM 87131-0001, USA*

Received 25 October 2005; revised 2 January 2006; accepted 6 January 2006

Abstract

Titania- and alumina-supported Au nanoparticles were synthesized by a deposition-precipitation method and subsequent thermal treatment in He. X-ray absorption spectroscopy at the Au-L_{III} edge revealed that the as-prepared Au/TiO_2 sample contained cationic Au that was reduced to a predominately metallic state after treatment in He at 623 K. Scanning transmission electron microscopy showed the Au to be highly dispersed over both the metal oxides, with an average particle size of 3.3 nm for Au/TiO_2 and 2.5 nm for Au/Al_2O_3. The global rate, apparent activation energy, and orders of reaction with respect to CO and O_2 of CO oxidation were different for the two metal oxide-supported samples. Steady-state isotopic transient kinetic analysis was used to explore the intrinsic turnover frequency (TOF_{intr}) and coverage of active carbon-containing intermediates (θ_{CO_x}) that led to carbon dioxide during CO oxidation. After correcting for CO_2 readsorption, the TOF_{intr} was found to be independent of temperature, approximately 3.4 s^{-1} for Au/TiO_2 (261–303 K) and 2.1 s^{-1} for Au/Al_2O_3 (272–343 K). At 293 K, the coverage of active carbon-containing intermediates was greater over Au/TiO_2 than over Au/Al_2O_3. The higher coverage of species-forming product on Au/TiO_2 is attributed to the greater availability of active surface oxygen on a titania catalyst compared with an alumina catalyst.

Keywords: Gold; Isotopic transient analysis; Titania; Alumina; Carbon monoxide; Oxidation of; Carbon dioxide; STEM; XANES; Oxygen

1. Introduction

Because bulk gold is considered the least reactive metal [1], its use in heterogeneous catalysis has traditionally been very limited. In 1989, interest in gold catalysis was prompted by Haruta et al. [2] when they reported the unique property of supported gold to effectively catalyze oxidation reactions at ambient temperature. Although understanding of gold catalysis has increased considerably, unresolved questions remain. One ongoing debate is about the role of metal oxide support in the low-temperature oxidation of CO over Au nanoparticles.

Some researchers have proposed that the primary role of metal oxide is merely to disperse the gold [3,4]. However, it has been documented that differing kinetics of CO oxidation are observed when gold nanoparticles are supported on different metal oxides [5–7]. Although the metal oxide can affect the size of the gold particles depending on the preparation method used, Wolf and Schüth [6] observed a higher rate of CO oxidation over a Au/TiO_2 sample than over a Au/Al_2O_3 sample with a similar gold particle size distribution. Conversely, Okumura et al. [4] prepared highly dispersed gold particles using a gas-phase grafting technique on Al_2O_3, TiO_2, SiO_2, and MCM-41 and observed a very similar TOF (based on surface gold atoms) for CO oxidation over each sample [4]. However, the samples that they prepared with SiO_2–Al_2O_3 (acidic support) and activated carbon (nonmetal oxide support) had a significantly lower TOF.

Although metal oxide seems to exert some effect on supported Au catalysts, different roles of the support have been proposed. Researchers studying model Au/MgO systems have hypothesized that oxygen-vacancy F-center defects on MgO provide a partial electron transfer that activates the Au parti-

* Corresponding author.
E-mail address: rjd4f@virginia.edu (R.J. Davis).

0021-9517/$ – see front matter
doi:10.1016/j.jcat.2006.01.009

cles for CO oxidation [8–10]. Others have suggested that the support may provide adsorption sites for the reactants. Results from infrared spectroscopy and reaction kinetics are consistent with CO adsorbing on the Au and O_2 adsorbing on the titania support [11–13]. However, a distinction is often made between reducible and nonreducible oxides in terms of O_2 adsorption [5]. A reducible metal oxide such as TiO_2 or Fe_2O_3, which can absorb a significant quantity of O_2, is thought to act as an oxygen source for CO oxidation, whereas a nonreducible metal oxide such as Al_2O_3 or SiO_2 is not considered important in the catalytic cycle because O_2 adsorption is much less favorable [5].

In this work, we performed an isotopic transient analysis (ITA) of CO oxidation over titania and alumina-supported gold catalysts. Our approach allowed a direct comparison of a reducible and a nonreducible metal oxide support on the intrinsic kinetics of CO oxidation. Isotopic transient analysis is used to determine a TOF based on the number of active intermediates on an operating catalyst. The ITA experiment involves making a step change in the isotopic content of one of the reactants (CO in this case) at steady-state reaction conditions. The pressure, temperature, total flow rate, and product composition are maintained during this change. Therefore, in the absence of isotopic mass effects, the steady-state reaction is not altered during the isotope switch. The transient response of the isotopically labeled product (CO_2) is monitored by mass spectroscopy. This transient response is used to determine the surface coverage (θ_{CO_x}) and the mean residence time (τ) of adsorbed carbon-containing intermediates that lead to CO_2. Shannon and Goodwin [14] have provided a more detailed description of the theory underlying this technique, and Efstathiou and Verykios have reviewed applications of the method to various reaction systems [15].

Isotopic transient analysis involves the characterization of *active* intermediates that lead to CO_2. If product CO_2 readsorbs on either active or inactive surface sites before leaving the catalyst bed, the measured residence time will be increased. Because CO_2 is known to adsorb on TiO_2 and Al_2O_3 [16], it is critical that τ be corrected for product readsorption. Furthermore, the work of Liu et al. [11,17] with Au on Ti and Fe hydroxides indicates that once CO_2 is formed, it exchanges oxygen with the support. Secondary reactions, such as oxygen exchange, would also affect the isotopic transient analysis, leading to overestimation of τ. Earlier, we reported the results from a preliminary isotopic transient investigation of CO oxidation over an alumina-supported gold catalyst [18]. Herein, we present a comparison of the oxidation of CO over Au/Al_2O_3 and Au/TiO_2 with an improved analysis of product readsorption and secondary reactions.

2. Experimental

2.1. Catalyst preparation

A deposition–precipitation method adapted from a previous report [19] was used to synthesize the catalysts in this study. Initially, 96 mL of a 9.6 mM $HAuCl_4$ (Aldrich, 99.9+%) aqueous solution was heated to 343 K and adjusted with dropwise addition of aqueous NaOH (Mallinckrodt, 98.6%) solution to pH 7. The gold solution was then added to a second flask containing 6 g of TiO_2 (Degussa, P-25) or Al_2O_3 (Mager Scientific, AP-312) suspended in 150 mL of distilled, deionized water also at 343 K. After stirring the mixture for 2 h, the solution was removed by suction filtration, and the catalyst was resuspended in 120 mL of distilled, deionized water at 343 K for 20 min. The process of filtering and resuspending in H_2O was repeated 3 additional times. After the final filtration, the catalyst was dried in air at 310 K for 24 h. The Au content of the catalysts was 1.22 wt% for Au/TiO_2 and 1.08 wt% for Au/Al_2O_3, as reported by Galbraith Laboratories (Knoxville, TN).

2.2. X-Ray absorption spectroscopy

The X-ray absorption spectra at the Au-L_{III} edge were recorded on beam line X-10C at the National Synchrotron Light Source, Brookhaven National Laboratory, Upton, NY. The storage ring operated at 2.8 GeV with currents ranging from 150 to 300 mA. Several Au containing compounds, Au_2O_3, $AuCl_3$, and AuCl (all from Alfa Aesar, 99.99%), were used as Au references with different formal oxidation states. The reference compounds were diluted with BN powder (Alfa Aesar, 99.5%) and pressed into self-supporting wafers. A light-tight Au foil (0.005 mm thick, Goodfellow, 99.9%) was used as a metallic Au reference. The spectra of the reference compounds and the Au foil were collected in transmission mode in air at ambient temperature. The spectra of the catalyst samples were collected in fluorescence mode as a result of their low Au content. A cell capable of heating and cooling the sample in a controlled atmosphere was used to allow characterization in an environment consistent with the reactor studies.

2.3. Scanning transmission electron microscopy

High-angle annular dark field (HAADF) imaging was performed using a JEOL 2010F microscope, operated at 200 kV. The catalyst samples were suspended in ethanol by lightly grinding them in an agate mortar and pestle, and deposited on a holey carbon support film on Cu TEM grids. The images were recorded using Digital Micrograph software and analyzed to determine particle size distributions. A probe size of approximately 0.3 nm was used for imaging, allowing easy resolution of particles <1 nm in diameter.

2.4. Isotopic transient and global kinetic measurements

Between 0.045 and 0.160 g of catalyst (−200/+100 mesh) was mixed with 0.3 to 0.525 g of SiC (Universal Photonics, 120 mesh) and loaded into a quartz tubular reactor. Before kinetic studies, the catalyst samples were treated at 623 K for 4 h under flowing He (99.999%, Messer, further purified by a Supelco OMI-2 filter). The samples were cooled in flowing He to the temperature of interest before admitting the reactant

gases: ^{12}CO (99.997%, Messer), O_2 (99.999%, BOC Gases), He (99.999%, Messer, further purified by a Supelco OMI-2 filter), and Ar (99.999%, Messer, further purified by a Supelco OMI-2 filter) to the reactor. The mole percentages of the reactant stream He:CO:O_2:Ar were 95.3:2:2:0.7. Carbon dioxide (99.999%, BOC Gases) was cofed with the reactants, as discussed below. All of the gases except Ar and cofed CO_2 were additionally purified by passage through a silica gel trap (Davisil Grade 635, Type 60A, 60–100 mesh) held at dry ice–acetone temperature. Total volumetric gas flow rates of 250–382 mL min^{-1} were used, yielding space velocities of approximately 1500–8500 mL min^{-1} g_{cat}^{-1}. Gases were supplied via mass flow controllers and back-pressure regulators ensured that all reactant streams and vent lines were maintained at 1.2 atm. All data were collected after at least 36 h time on stream. The CO oxidation activity of the World Gold Council reference Au/TiO_2 #02-5 (WGC Au/TiO_2) was evaluated for comparison. The WGC Au/TiO_2 had a Au particle size distribution of 3.7 ± 0.8 nm and a Au loading of 1.47 wt% as reported by the World Gold Council.

Schematic representations of the apparatus are given in Figs. 1a and b. The flow arrangement of Fig. 1a was utilized while performing the isotopic transient analysis of CO oxidation. This setup allowed a step change in isotopically labeled carbon monoxide. The isotopic switch was accomplished by injecting a known volume of ^{13}CO (Cambridge Isotopes, 99.5% CO, 98+% ^{16}O, 99+% ^{13}C, further purified with a cold silica gel trap) and He into the feed stream containing ^{12}CO and Ar. Argon was mixed with the ^{12}CO as an inert gas tracer. Because Ar was not present in the injection volume, the decay of the Ar signal was used to quantify the gas-phase holdup of the system. The flow arrangement of Fig. 1b was used to determine the contribution of CO_2 readsorption and secondary reactions without the presence of CO. This arrangement allowed a step change in CO_2 concentration permitting transient analysis of CO_2 on the catalyst surface while maintaining a background concentration of CO_2 in the feed. The step change in CO_2 concentration was obtained by injecting a volume of He into a stream of CO_2 and Ar. Again, the Ar was used to determine the gas-phase holdup of the system.

A Balzers–Pfieffer Prisma 200 amu mass spectrometer monitored the concentrations of Ar, $^{12}CO_2$, and $^{13}CO_2$ ($m/e = 40$, 44, and 45, respectively) continuously. The lines from the reactor effluent to the mass spectrometer as well as the mass spectrometer housing were heated to approximately 443 K. Multiple switches ($^{12}CO/Ar \rightarrow {}^{13}CO/He$ or $^{12}CO_2/Ar \rightarrow He$) were recorded at each set of experimental conditions.

The composition of the reactor effluent was also analyzed using the mass spectrometer while exploring the effect of temperature and reactant partial pressure on the global rate of CO oxidation. Gas feeds of known composition were used to generate calibration factors to determine the molar compositions of He, O_2, CO, Ar, and CO_2.

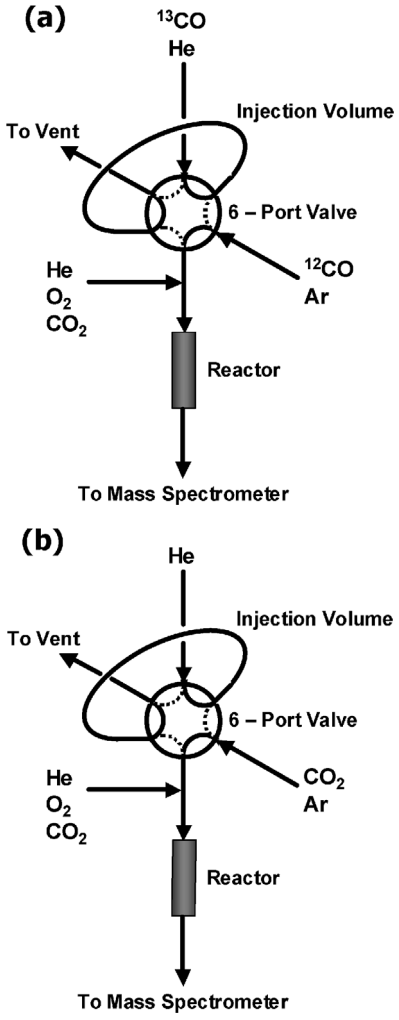

Fig. 1. Schematic representations of the reactor system (a) for CO isotopic transient analysis and (b) CO_2 transient analysis.

3. Results and discussion

3.1. X-Ray absorption spectroscopy

The oxidation state of the supported Au was determined using X-ray absorption spectroscopy (XAS) by comparing the spectra of the catalysts to those of the Au reference compounds. Fig. 2 shows the X-ray absorption near-edge structure (XANES) of the Au reference compounds in different oxidation states. Absorption at the L_{III}-edge corresponds to the excitation of $2p_{3/2}$ electrons to unoccupied d states above the Fermi level [20]. Compounds such as Au_2O_3 and $AuCl_3$, which contain Au in the +3 formal oxidation state, have many unoccupied d states resulting in a relatively large absorption peak at the L_{III}-edge, although AuCl, which contains Au in the +1 formal oxidation state, has fewer unoccupied d states, resulting in a smaller absorption peak. Although the electronic structure of zero valent Au is $5d^{10}6s^1$, hybridization with 6s and 6p states in the solid results in a finite density of unoccupied d states [20]. These unoccupied d states are observed as a small shoulder at the L_{III}-edge for Au foil.

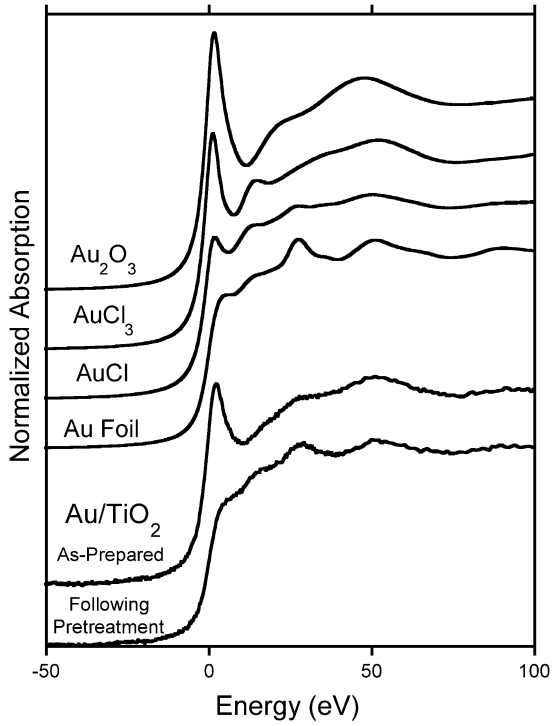

Fig. 2. X-Ray absorption near edge spectra at the Au-L_{III} edge of Au reference compounds and Au/TiO_2 sample in He. Spectra are offset for clarity. The energies are defined relative to the first inflection point in the L_{III}-edge of Au foil.

Also included in Fig. 2 is the change of the Au/TiO_2 XANES with thermal pretreatment in He. At ambient temperature in He, the as-prepared Au/TiO_2 appeared to contain cationic Au, as a peak of intermediate intensity is present at the absorption edge. After treatment in He at 623 K, the highest temperature of the catalyst pretreatment, essentially all of the Au was reduced to the metallic state. Poor data quality did not allow accurate estimation of the Au particle size from the EXAFS data. Previously, we reported the results of XAS characterization of a similar Au/Al_2O_3 catalyst [18]. In that study, we found the as-prepared Au/Al_2O_3 contained Au in a +3 oxidation state. When the sample was heated in He from 298 to 623 K, the conditions of the catalyst pretreatment, the Au autoreduced to a predominately metallic state.

The catalysts were synthesized with a deposition–precipitation method using $HAuCl_4$ as the metal precursor. The precursor would hydrolyze to form $[Au(OH)_xCl_{4-x}]^-$, with x close to 3 at the pH value of 7 used in the preparation [19]. It is likely that the supported Au was initially in the form of $Au(OH)_3$ [19]. The peak at the Au-L_{III} absorption edge of the as-prepared Au/TiO_2 (Fig. 2) indicates the presence of cationic Au. The peak is of intermediate intensity suggesting there was a mixture of Au^0, Au^{1+}, and/or Au^{3+}. It is likely that the mild drying conditions of the sample preparation promoted autoreduction of the Au on TiO_2. These results are consistent with the observation of more facile reduction of Au on TiO_2 compared with Al_2O_3 [21,22]. The lack of any discernible peak at the absorption edge after treatment in He at 623 K indicates that the Au on TiO_2 and Al_2O_3 [18] was reduced to Au^0; therefore, the active catalysts appeared to contain predominately metallic Au. This is consistent with other researchers characterizing the Au oxidation state of active CO oxidation catalysts using X-ray absorption and Mössbauer spectroscopy [21–25].

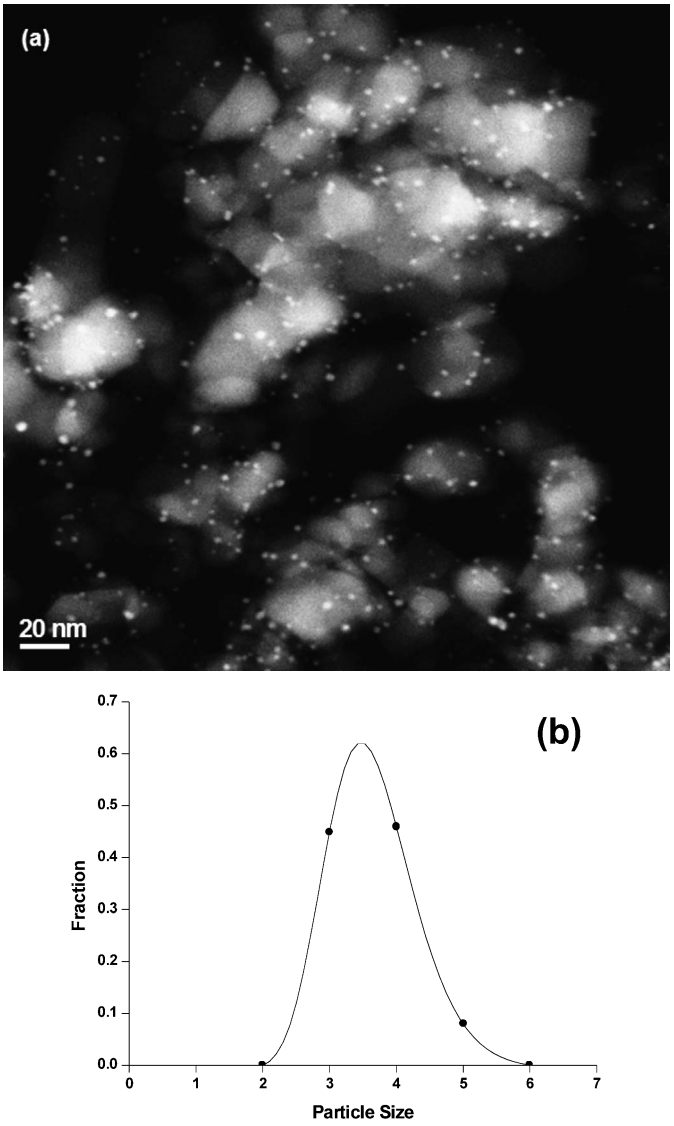

Fig. 3. STEM (a) image and (b) Au particle size distribution of Au/TiO_2 fit to a log normal distribution.

3.2. Scanning transmission electron microscopy

The HAADF STEM images of the samples (Figs. 3a and 4a) show well-dispersed, uniform gold nanoparticles. From STEM images, an average particle size was calculated by measuring approximately 300 particles using Digital Micrograph software. The particle size distributions for these samples are shown in Figs. 3b and 4b. In all cases, the size distributions could be well fitted to a lognormal distribution.

Because the same technique and conditions were used to prepare the Au/TiO_2 and Au/Al_2O_3 of this study, the metal oxide was the significant variable in the preparation. One difference between the metal oxide supports is the isoelectric point, which

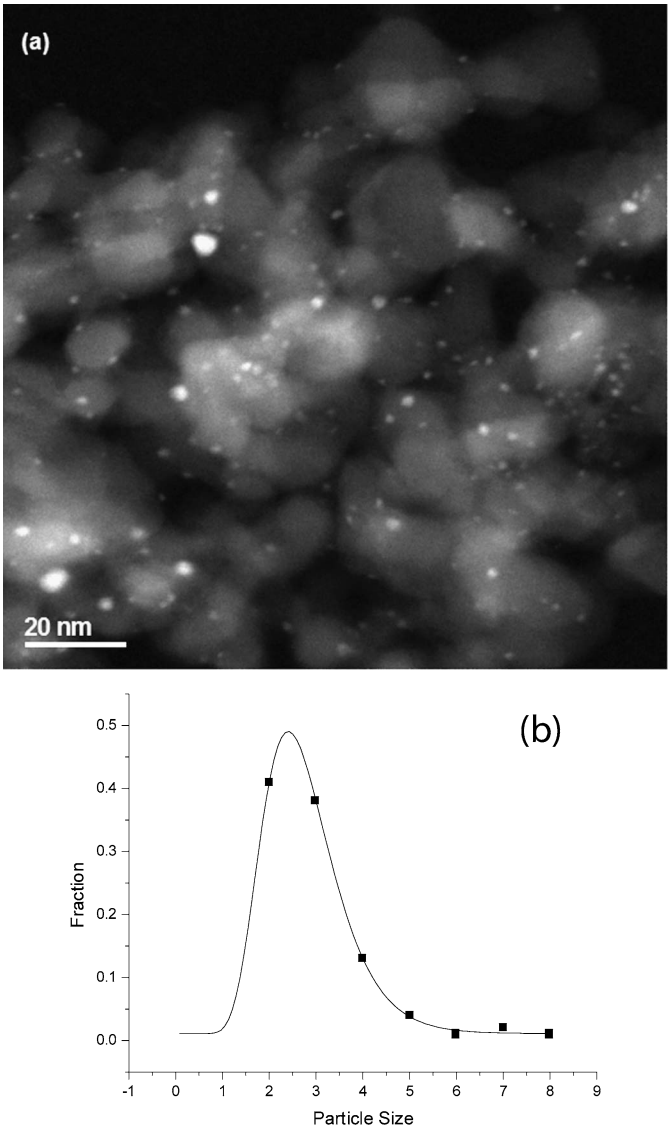

Fig. 4. STEM (a) image and (b) Au particle size distribution of Au/Al_2O_3 fit to a log normal distribution.

is approximately 6 for TiO_2 and 8 for Al_2O_3 [26]. The relationship between the pH during precipitation, the isoelectric point of the metal oxide, and the activity for CO oxidation were demonstrated by Wolf and Schüth [6]. They observed that as the pH during precipitation was increased, the activity for CO oxidation increased, which correlated with a decrease in the Au particle size. This trend was observed until the pH was increased past the isoelectric point of the metal oxide, at which point the amount of Au deposited decreased. With the preparation conditions used in our work, the average Au particle size (3.3 ± 0.5 for Au/TiO_2 and 2.5 ± 1.1 nm for Au/Al_2O_3) and loading (1.22 wt% for Au/TiO_2 and 1.08 wt% for Au/Al_2O_3) were similar on both supports. Therefore, it is assumed that differences in the kinetics of CO oxidation observed in this study are attributed to the nature of the metal oxide support without significant contributions induced through the catalyst preparation.

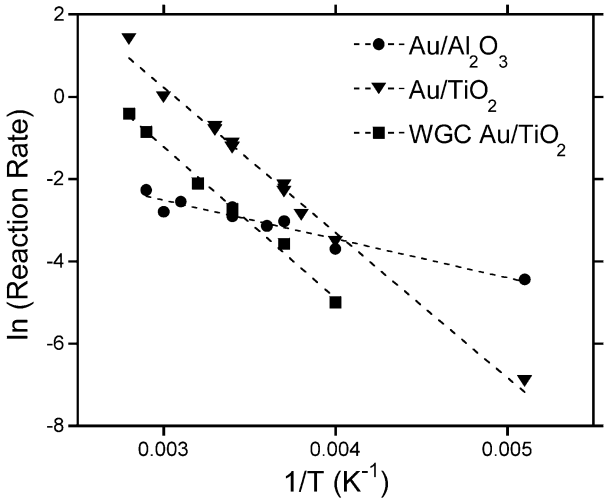

Fig. 5. Arrhenius-type plots for CO oxidation ($He:CO:O_2:Ar = 95.3:2:2:0.7$) over WGC Au/TiO_2, Au/TiO_2, and Au/Al_2O_3. Dashed lines represent linear regression of the data used to calculate apparent activation energies. The units of reaction rate are $mol_{CO_2}\, mol_{Au}^{-1}\, s^{-1}$.

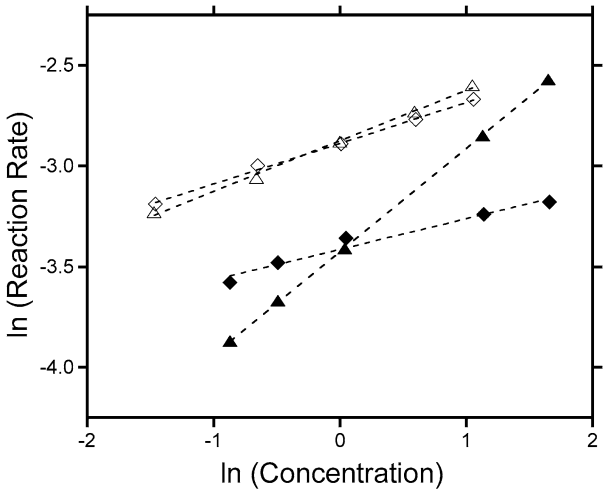

Fig. 6. Effect of reactant concentration on the rate of reaction at 273 K; diamonds represent variation of CO concentration while maintaining the O_2 concentration at 1.0 mol%, triangles represent variation of O_2 concentration while maintaining the CO concentration at 1.0 mol%. Filled symbols are for Au/Al_2O_3, open symbols are for Au/TiO_2. Dashed lines represent linear regression of the data used to calculate orders of reaction. The units of reaction rate are $mol_{CO_2}\, mol_{Au}^{-1}\, s^{-1}$.

3.3. Global kinetics of CO oxidation

The Arrhenius-type plots of CO oxidation over Au/TiO_2 and Au/Al_2O_3 are presented in Fig. 5. The World Gold Council reference Au/TiO_2 (WGC Au/TiO_2) was also evaluated for CO oxidation activity and is shown in Fig. 5. The effect of reactant partial pressure on the global reaction rate at 273 K is presented in Fig. 6. The fractional conversion of CO was less than 0.2 over Au/Al_2O_3 at all temperatures studied. For Au/TiO_2, the fractional conversion of CO was $\leqslant 0.2$ at 261 and 273 K and $\leqslant 0.37$ at 293 and 303 K. The estimated apparent activation energies (E_a) and orders of reaction with respect to CO and O_2 are presented in Table 1. Also included in Table 1 are turnover

Table 1
Kinetic results during CO oxidation at 273 K[a]

Sample	TOF[b] (s^{-1})	E_a (kJ mol^{-1})	Orders of reaction		Refs.
			O_2	CO	
Au/TiO_2	0.34	29	0.25	0.20	This work
WGC[c]	0.10	31	–	–	This work
	0.13	34	0.24	0.05	[27]
	–	29	0.02	0.41	[12]
	–	–	0.32	0.34	[28]
Au/Al_2O_3	0.18	8	0.52	0.15	This work
	0.03	32	–	–	[4]

[a] Data were collected at 273 K except for Ref. [28] which were collected at 343 K.
[b] TOF is the global reaction rate per Au atom in the catalyst normalized by the fraction of metal exposed.
[c] World Gold Council Au/TiO_2 #02-5 reference catalyst.

frequencies (TOFs) calculated by dividing the global reaction rate by the dispersion of Au. The fraction of Au exposed was estimated from the inverse of the surface-average Au particle size determined by STEM (3.4 nm for Au/TiO_2 and 3.8 nm for Au/Al_2O_3), corresponding to a dispersion of 29% for Au/TiO_2 and 26% for Au/Al_2O_3. Table 1 also includes selected published results for comparison.

From the Arrhenius-type plots of Fig. 5, a difference in the apparent activation energy of CO oxidation over Au/TiO_2 and Au/Al_2O_3 is clear. At approximately 245 K, the rate is the same over both samples. Above 245 K, the Au/TiO_2 has a higher global rate, whereas below 245 K, the Au/Al_2O_3 is more active. This is reflected in the greater apparent activation energy observed for Au/TiO_2 compared with Au/Al_2O_3 (29 vs. 8 kJ mol^{-1}, respectively). The higher activity of titania-supported Au compared with alumina-supported Au for CO oxidation above 245 K is consistent with observations reported in the literature [4,27]. The apparent activation energy for CO oxidation over the Au/TiO_2 of this study was consistent with the WGC Au/TiO_2 and values reported elsewhere [12,27]. However, the apparent activation energy observed for Au/Al_2O_3 in this work was lower than that reported by Okumura et al. [4] (8 vs. 32 kJ mol^{-1}, respectively). The low positive orders of reaction with respect to O_2 and CO for CO oxidation were observed for both samples of this study. The order with respect to O_2 over Au/Al_2O_3 was twice that of Au/TiO_2 (0.52 vs. 0.25, respectively). The order with respect to CO was similar over both samples (0.15 for Au/Al_2O_3 and 0.20 for Au/TiO_2). The orders of reaction for Au/TiO_2 are comparable to those reported elsewhere [12,27,28]. Although orders of reaction for CO oxidation over Au/Al_2O_3 have not been reported in the literature, they are similar to those reported for Au/TiO_2. The slight dependence of the reaction rate on the reactant partial pressures suggests that the adsorption of O_2 and CO is not highly competitive as a result of separate adsorption sites [12,13] and/or very low surface coverages [29–33].

3.4. Isotopic transient analysis

Isotopic transient analysis of CO oxidation was performed to explore the effect of metal oxide support on the mean residence time and coverage of active carbon-containing intermediates leading to CO_2. A typical set of carbon dioxide and argon transients after a switch between ^{12}CO/Ar and ^{13}CO/He are shown in Fig. 7.

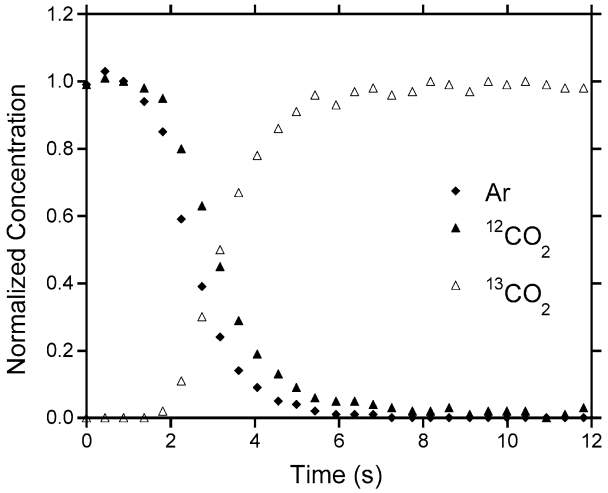

Fig. 7. Example of an isotopic transient during CO oxidation over Au/TiO_2 at 303 K.

The average residence time of surface intermediates (τ) leading from CO (the isotopically labeled reactant) to CO_2 is calculated by integrating the area between the normalized transients of $^{12}CO_2$ ($F_{^{12}CO_2}$) or $^{13}CO_2$ ($1 - F_{^{13}CO_2}$) and Ar (F_{Ar}),

$$\tau = \int_0^\infty \left[F_{^{12}CO_2} - F_{Ar}\right] dt. \quad (1)$$

Because τ is calculated using the transient response of the product, the observed value can include contributions from readsorption or secondary reactions of CO_2. These phenomena will result in an artificially higher value of τ that does not reflect the intrinsic kinetics of the CO oxidation reaction. Readsorption of CO_2 was anticipated because both Al_2O_3 and TiO_2 have acidic and basic surface sites [16]. In addition, oxygen exchange of CO_2 with the support is suggested by Liu et al. who performed isotopic studies of CO oxidation over Au supported on Ti and Fe hydroxides [11,17]. Methods to correct for product readsorption have been presented by Ali and Goodwin [34]. One approach to account for CO_2 readsorption is to measure τ at various flow rates. In doing so, the residence time of CO_2 in the reactor is altered, thus changing the likelihood of readsorption. Readsorption of the product is negligible if τ is independent of flow rate. However, a positive relationship of τ with inverse flow rate indicates that interparticle readsorption of the product may be occurring. Extrapolating τ to zero inverse flow rate or zero residence time adjusts for interparticle readsorption. Although this extrapolation provides a better estimate of τ, the method does not account for readsorption within the catalyst pores. An approach to account for intraparticle readsorption is to cofeed unlabeled product [34]. The cofed product competitively adsorbs with that formed catalytically, thus reducing the contribution of readsorption to the observed τ. In theory, τ will approach a value that represents intrinsic kinetics with

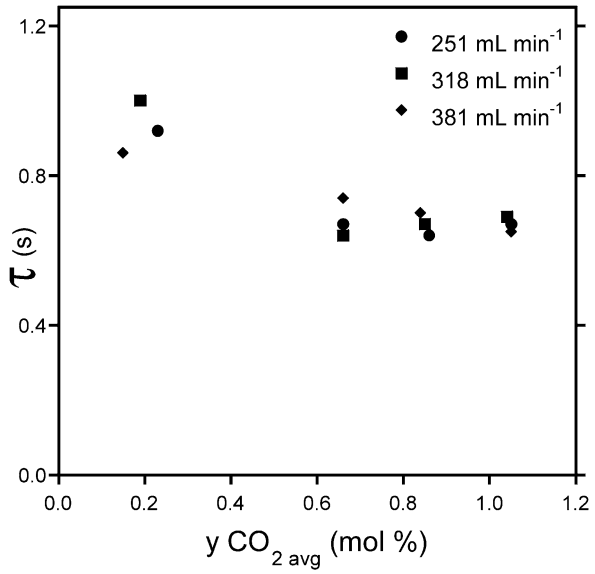

Fig. 8. Effect of flow rate on measured τ over Au/TiO_2 at 293 K with varying levels of co-fed CO_2 to the reactor. The mole fraction of CO_2 in the reactor, $y_{CO_2\ avg}$, was the average of the inlet and outlet mole fractions.

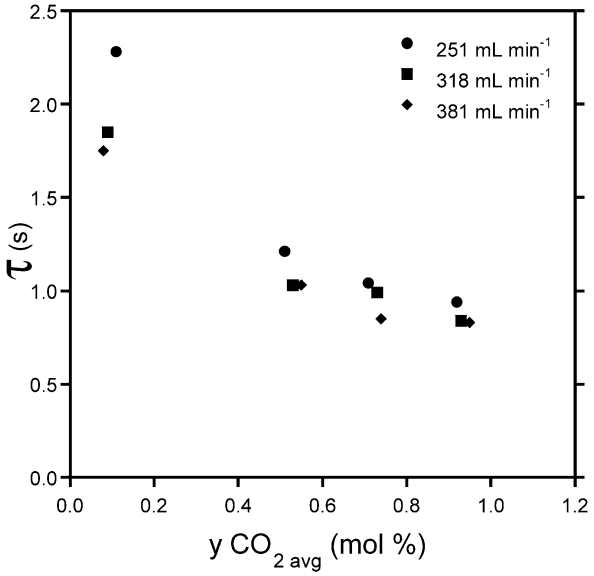

Fig. 9. Effect of flow rate on measured τ over Au/Al_2O_3 at 323 K with varying levels of co-fed CO_2 to the reactor. The mole fraction of CO_2 in the reactor, $y_{CO_2\ avg}$, was the average of the inlet and outlet mole fractions.

increasing cofed product concentration. The concentration of cofed product should be sufficient such that τ is independent of product concentration. This indicates adequate competitive adsorption is present to account for intraparticle readsorption. However, care must be taken not to influence the kinetics of the probe reaction through the introduction of excess product. The techniques described above to account for product readsorption were applied in this study. A <25% change in the global rate was observed with the addition of cofed CO_2.

The reactor was loaded with different amounts of catalyst for the two higher and two lower temperatures in an attempt to maintain differential conversion. The τ values observed from the isotopic transient measurements, as a function of average CO_2 concentration, are presented in Figs. 8 and 9, for Au/TiO_2 (293 K) and Au/Al_2O_3 (323 K), respectively. The reported τ values are an average of four switches between ^{12}CO and ^{13}CO using both the $^{12}CO_2$ and $^{13}CO_2$ ($m/e = 44$ and 45, respectively) signals. The average standard deviation of τ at each set of experimental conditions was 0.10 s for Au/TiO_2 and 0.13 s for Au/Al_2O_3. The average CO_2 concentration ($y_{CO_2\ avg}$) was calculated as the average of the inlet and outlet molar CO_2 concentration.

For both samples (Figs. 8 and 9), a decrease in τ was observed as the concentration of cofed CO_2 was increased. Above an average CO_2 concentration of approximately 0.6 mol%, τ was nearly independent of CO_2 concentration. Figs. 8 and 9 also illustrate the influence of total gas flow rate on the observed τ. As discussed by Ali and Goodwin [34], a decrease in τ with an increase in total gas flow rate is strong evidence for interparticle readsorption of product along the catalyst bed. For example, artifacts of interparticle readsorption of CO_2 are found in the τ values associated with the lowest average CO_2 concentration in Figs. 8 and 9. However, cofeeding CO_2 ($y_{CO_2\ avg} > 0.6$ mol%) minimized those artifacts. For each sample, the effects of flow rate and average CO_2 concentration were similar at the other temperatures of this study (not shown). The complete set of results is presented in the supplementary material. The transient of ^{12}CO was also measured during CO oxidation and found to nearly match that of the Ar transient ($\tau < 0.14$ s). Therefore, the exchange of CO isotopes within the reactor system does not significantly contribute to the observed CO_2 transient.

To estimate the contribution of readsorption and secondary reactions of CO_2 that may have been present during the isotopic transient analysis of CO oxidation, CO_2 switching experiments were performed without the presence of CO. These experiments involved making a 0.2 mol% step change in the CO_2 concentration while simultaneously cofeeding 0.8 mol% CO_2 over the catalyst sample. This was done while maintaining the same O_2 concentration, total gas flow rate, pressure, and temperature used during the isotopic transient studies. The difference between the isotopic transient data collected with CO oxidation and the CO_2 transient data collected without reaction would be attributed to the oxidation of CO.

Representative examples of the data collected without CO oxidation (labeled “without reaction”), as well as those data from the isotopic transient analysis of CO oxidation (labeled “with reaction”) are presented in Figs. 10 and 11 for Au/TiO_2 and Au/Al_2O_3, respectively. The reaction temperatures associated with Figs. 10 and 11 are the same as those in Figs. 8 and 9. The τ data are presented as a function of inverse flow rate to demonstrate the influence of interparticle readsorption and are at a 0.9 mol% average CO_2 concentration, to represent a uniform correction of intraparticle readsorption. The isotopic transient τ values (with CO oxidation) were determined by performing a linear regression of the τ data as a function of $y_{CO_2\ avg}$ (at $y_{CO_2\ avg} > 0.4\%$), then calculating τ at an $y_{CO_2\ avg}$ value of 0.9 mol%. The CO_2 transient data were determined at $yCO_2\ avg$ of 0.9 mol% and thus were used as measured.

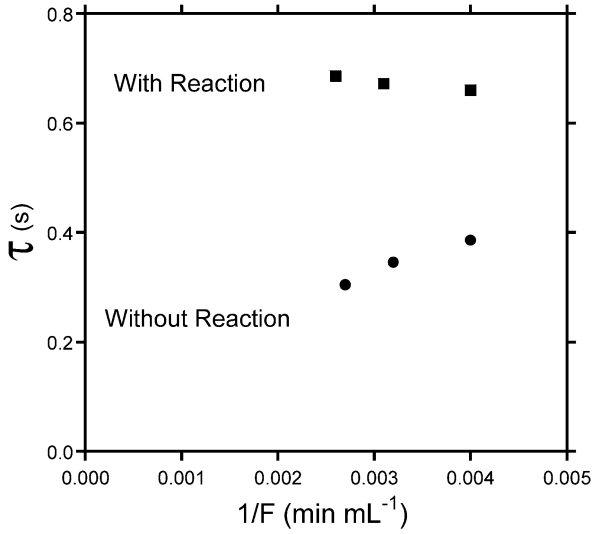

Fig. 10. Effect of flow rate on τ at $y_{CO_2\ avg} = 0.9$ mol% at 293 K and 1.2 atm over Au/TiO_2. 'With Reaction' are isotopic transient data of CO oxidation; 'Without Reaction' are CO_2 transient data without CO oxidation.

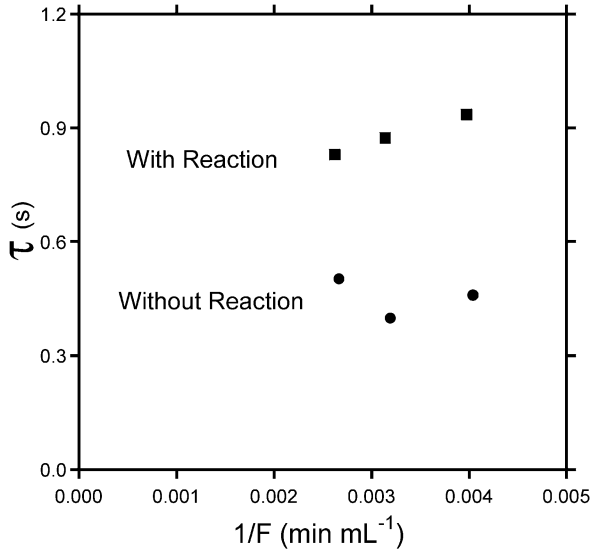

Fig. 11. Effect of flow rate on τ at $y_{CO_2\ avg} = 0.9$ mol% at 323 K and 1.2 atm over Au/Al_2O_3. 'With Reaction' are isotopic transient data of CO oxidation; 'Without Reaction' are CO_2 transient data without CO oxidation.

Figs. 10 and 11 clearly show that contributions to τ not associated with the oxidation reaction were observed during the isotopic transient analysis of CO oxidation over both Au/TiO_2 and Au/Al_2O_3. To estimate the average residence time of *active* surface intermediates leading to CO_2, the difference in τ with and without CO oxidation was calculated. This was done by averaging τ at the three flow rates and subtracting the average τ value without reaction from the average τ value with CO oxidation,

$$\Delta\tau = \bar{\tau}_{\text{w/CO oxidation}} - \bar{\tau}_{\text{w/o reaction}}. \tag{2}$$

Thus, $\Delta\tau$ represents the residence time of active carbon-containing intermediates involved in the oxidation of CO. These values are presented in Table 2 for the various temperatures. Isotopic transient analysis of CO oxidation below the temperatures reported here was hindered by excessive CO_2 readsorption.

The value of τ corrected for CO_2 readsorption ($\Delta\tau$) is a good approximation of the intrinsic activity of the catalytic sites, as determined by

$$\text{TOF}_{\text{intr}} = 1/\Delta\tau. \tag{3}$$

The intrinsic TOF (TOF_{intr}), as defined by Eq. (3), provides an upper bound because it is based on the actual surface concentration of intermediates under reaction conditions. The classical calculation of TOF involves the total number of surface metal atoms. Because not all of the surface atoms may participate in the reaction, the conventional TOF provides a lower bound on the normalized rate. Conversely, if the active surface sites are not saturated at the time of the isotopic switch, then TOF_{intr} will be greater than the true TOF of the catalytic sites. The moles of reactive surface intermediates per mole of Au, N_{CO_x}, was calculated using the following steady-state mass balance:

$$N_{CO_x} = \Delta\tau \times R_{CO_2}, \tag{4}$$

where R_{CO_2} is the steady-state rate of CO oxidation per mole of Au atoms. The surface coverage of reactive intermediates, θ_{CO_x}, can then be calculated from N_{CO_x} using the Au dispersion,

$$\theta_{CO_x} = \frac{N_{CO_x}}{\text{Au dispersion}}. \tag{5}$$

The global reaction rates, TOF_{intr}, and θ_{CO_x}, at the various temperatures are also included in Table 2.

After correcting for CO_2 readsorption/secondary reactions, it was discovered that τ was independent of temperature for both samples. An average TOF_{intr} of 3.4 s^{-1} for Au/TiO_2 and 2.1 s^{-1} for Au/Al_2O_3 was calculated. The temperature independence of the intrinsic rate suggests that the surface reaction of adsorbed CO with surface oxygen was nearly unactivated.

Using Eq. (5), the coverage of carbon-containing intermediates leading to CO_2 was found to actually increase with temperature. Therefore, it is unlikely that θ_{CO_x} is a function of the equilibrium adsorption of CO [30]. The value of θ_{CO_x} at 293 K was higher on the Au/TiO_2 compared with the Au/Al_2O_3, whereas it was the same on the two samples at 273 K. The absolute magnitude of θ_{CO_x} must be viewed cautiously because the adsorption of CO has also been observed on bare TiO_2 and Al_2O_3 [30,35] and the calculation of θ_{CO_x} assumes that Au is the only active surface. More informative is the relative value of θ_{COx} that indicates more carbon-containing intermediates are found on Au/TiO_2 compared with Au/Al_2O_3 at higher temperatures, which is related to the higher observed activation energy on Au/TiO_2.

The Au/TiO_2 had a higher global reaction rate over the temperature range of this study. The higher global rate was the result of both a higher TOF_{intr} and a greater number of active intermediates, suggesting that the metal oxide may influence the oxidation of CO through different means. Two general roles of the metal oxide support have been proposed: (1) to influence the electronic properties of the Au nanoparticles and (2) to supply adsorption sites.

Table 2
Isotopic transient results during CO oxidation[a]

Sample	T (K)	Global reaction rate ($mol_{CO_2}\ mol_{Au}^{-1}\ s^{-1}$)	τ (s) w/ reaction	τ (s) w/o reaction	$\Delta\tau$[b] (s)	TOF_{intr}[c] (s^{-1})	θ_{CO_x}[d]
Au/TiO_2	303	0.44	0.62	0.37	0.25	4.1	0.38
	293	0.32	0.67	0.35	0.32	3.1	0.36
	273	0.10	0.87	0.60	0.27	3.7	0.09
	261	0.06	0.94	0.59	0.35	2.8	0.07
Au/Al_2O_3	343	0.10	0.92	0.41	0.51	2.0	0.20
	323	0.08	0.88	0.45	0.43	2.3	0.13
	292	0.07	1.22	0.73	0.49	2.0	0.13
	272	0.05	1.39	0.86	0.52	1.9	0.10

[a] Experimental conditions: 1.2 atm total pressure; $He:CO:O_2:Ar = 95.3:2:2:0.7$.
[b] Difference between τ with and without CO oxidation.
[c] Defined as $\Delta\tau^{-1}$.
[d] Fractional Au coverage of active intermediates based on 29 and 26% Au dispersions for Au/TiO_2 and Au/Al_2O_3, respectively.

It is possible that an electronic effect generated by the metal oxide on Au nanoparticles would result in the difference in TOF_{intr} observed for CO oxidation over the Au/TiO_2 and Au/Al_2O_3. However, no attempt to resolve a direct observation of an electronic effect was made in this work. Nonetheless, the results obtained by other researchers performing experimental and theoretical studies of Au supported on MgO and TiO_2 have lead to the suggestion that F-centers in the metal oxide play an important role in CO oxidation [8–10,36–38]. Goodman et al. [9] showed a correlation between the relative concentration of F-centers in MgO and the activity of Au/MgO catalysts for CO oxidation. The F-centers are believed to electronically alter the Au nanoparticles through charge transfer, allowing the activation of O_2 [8,38]. Arrii et al. [7] synthesized Au nanoparticles of similar size distributions on Al_2O_3, ZrO_2, and TiO_2 via a laser vaporization technique. From X-ray photoelectron spectroscopy results, they determined the presence of metal–support interactions. However, the extent of the interaction did not correlate with the observed activity for CO oxidation over the different samples. Therefore, they suggested that the electronic effect is secondary to the nature of the support, which could influence the availability of reactant adsorption sites.

Differences in the ability of TiO_2 and Al_2O_3 to adsorb O_2 may provide insight into the behavior of θ_{CO_x}. The coverage of active carbon-containing intermediates leading to product was observed to increase with increasing temperature, indicating that θ_{CO_x} is not representative of the equilibrium adsorption of CO. Conceivably, θ_{CO_x} is a function of O_2 activation and the subsequent availability of active oxygen species. For example, as the temperature is increased, an increase in the rate of O_2 activation would lead to an increase in the number of active oxygen-containing intermediates. The greater availability of active oxygen would increase the amount of adsorbed CO that leads to product. Regarding O_2 adsorption, a distinction is often made between reducible (TiO_2) and nonreducible (Al_2O_3) metal oxides. Significant O_2 uptake is anticipated on reducible metal oxides, but not on nonreducible metal oxides [5,29,32]. More readily available O_2 provided by the TiO_2 versus Al_2O_3 (reducible vs. nonreducible metal oxide) correlates with the higher θ_{CO_x} observed over Au/TiO_2 compared with Au/Al_2O_3. This is also reflected in the lower order of reaction with respect to O_2 observed over Au/TiO_2 compared with Au/Al_2O_3.

Schubert et al. [5] prepared mixed-oxide-supported Au samples to explore the effect of reducible and nonreducible metal oxides on CO oxidation. They deposited gold on various compositions of $Fe_2O_3 \cdot MgO$ and tested the materials for CO oxidation. The TOF increased with increasing Fe_2O_3 content despite an increase in Au particle size. Results from time-resolved CO titrations over Fe_2O_3 and Au/Fe_2O_3 with preadsorbed O_2 suggest the Fe_2O_3 provided a readily available supply of O_2. They proposed that the ability of reducible metal oxides to supply oxygen promotes the activity of Au/reducible metal oxide systems compared with Au supported on nonreducible metal oxides [5]. Although the effect of the metal oxide on supported Au catalyzed CO oxidation is not completely understood, the metal oxide support appears to influence the availability and subsequent incorporation of oxygen into CO_2. Nevertheless, the activity of Au/TiO_2 and Au/Al_2O_3 is quite similar over the temperature range of this study.

4. Conclusions

Deposition–precipitation using $HAuCl_4$ followed by thermal treatment in He at 623 K was a viable technique for preparing similar Au dispersion and loading on TiO_2 and Al_2O_3. XAS indicated the Au was in a predominately metallic state on both metal oxides after thermal treatment in He. The overall activation energy and reaction orders for CO oxidation depended on the type of metal oxide support. Contributions of CO_2 readsorption and/or secondary reactions were observed during the isotopic transient analysis of CO oxidation despite cofeeding CO_2 to introduce competitive adsorption. After correcting for these effects, the TOF_{intr} was found to be independent of temperature, with values of 3.4 s^{-1} for Au/TiO_2 and 2.1 s^{-1} for Au/Al_2O_3. This finding suggests that reaction of CO with surface oxygen is a nearly unactivated process and is nearly independent of the support. However, the coverage of carbon-containing intermediates leading to product was observed to increase with temperature, which is inconsistent with the equilibrium adsorption of CO. Consequently, θ_{CO_x} is suspected to be a function of the availability and subsequent activation of O_2. The difference

in θ_{CO_x} observed over the two catalysts is possibly the result of different O_2 activation mechanisms induced by the reducibility of the metal oxide. Although the intrinsic rate of CO oxidation is nearly independent of the support, the ability of Au/metal oxide to activate O_2 is a key feature in determining the global reaction rate.

Acknowledgments

This work was supported by the National Science Foundation (grants CTS-0121619 and CTS-02-10835). The research was carried out partly at the National Synchrotron Light Source, Brookhaven National Laboratory, which is supported by the US Department of Energy, Division of Materials Sciences and Division of Chemical Sciences (contract DE-AC02 98CH10886).

Supplementary material

Supplementary material associated with this article can be found, in the online version, at doi:10.1016/j.jcat.2006.01.009.

References

[1] B. Hammer, J.K. Norskov, Nature 376 (1995) 238.
[2] M. Haruta, N. Yamada, T. Kobayashi, S. Iijima, J. Catal. 115 (1989) 301.
[3] N. Lopez, T.V.W. Janssens, B.S. Clausen, Y. Xu, M. Mavrikakis, T. Bligaard, J.K. Norskov, J. Catal. 223 (2004) 232.
[4] M. Okumura, S. Tsubota, M. Haruta, J. Mol. Catal. A 199 (2003) 73.
[5] M.M. Schubert, S. Hackenberg, A.C. van Veen, M. Muhler, V. Plzak, R.J. Behm, J. Catal. 197 (2001) 113.
[6] A. Wolf, F. Schüth, Appl. Catal. A 226 (2002) 1.
[7] S. Arrii, F. Morfin, A.J. Renouprez, J.L. Rousset, J. Am. Chem. Soc. 126 (2004) 1199.
[8] B. Yoon, H. Hakkinen, U. Landman, A.S. Worz, J.M. Antonietti, S. Abbet, K. Judai, U. Heiz, Science 307 (2005) 403.
[9] Z. Yan, S. Chinta, A.A. Mohamed, J.P. Fackler, D.W. Goodman, J. Am. Chem. Soc. 127 (2005) 1604.
[10] H. Hakkinen, W. Abbet, A. Sanchez, U. Heiz, U. Landman, Angew. Chem. Int. Ed. 42 (2003) 1297.
[11] H. Liu, A.I. Kozlov, A.P. Kozlova, T. Shido, K. Asakura, Y. Iwasawa, J. Catal. 185 (1999) 252.
[12] M.A. Bollinger, M.A. Vannice, Appl. Catal. B 8 (1996) 417.
[13] F. Boccuzzi, A. Chiorino, M. Manzoli, P. Lu, T. Akita, S. Ichikawa, M. Haruta, J. Catal. 202 (2001) 256.
[14] S.L. Shannon, J.G. Goodwin, Chem. Rev. 95 (1995) 677.
[15] A.M. Efstathiou, X.E. Verykios, Appl. Catal. A 151 (1997) 109.
[16] S.V. Bordawekar, E.J. Doskocil, R.J. Davis, Langmuir 14 (1998) 1734.
[17] H.C. Liu, A.I. Kozlov, A.P. Kozlova, T. Shido, Y. Iwasawa, Phys. Chem. Chem. Phys. 1 (1999) 2851.
[18] J.T. Calla, R.J. Davis, J. Phys. Chem. B 109 (2005) 2307.
[19] H.H. Kung, M.C. Kung, C.K. Costello, J. Catal. 216 (2003) 425.
[20] R.J. Davis, M. Boudart, J. Phys. Chem. 98 (1994) 5471.
[21] C.K. Costello, J. Guzman, J.H. Yang, Y.M. Wang, M.C. Kung, B.C. Gates, H.H. Kung, J. Phys. Chem. B 108 (2004) 12529.
[22] J.H. Yang, J.D. Henao, M.C. Raphulu, Y.M. Wang, T. Caputo, A.J. Groszek, M.C. Kung, M.S. Scurrell, J.T. Miller, H.H. Kung, J. Phys. Chem. B 109 (2005) 10319.
[23] J. Guzman, S. Kuba, J.C. Fierro-Gonzalez, B.C. Gates, Catal. Lett. 95 (2004) 77.
[24] V. Schwartz, D.R. Mullins, W.F. Yan, B. Chen, S. Dai, S.H. Overbury, J. Phys. Chem. B 108 (2004) 15782.
[25] A. Goossens, M.W.J. Craje, A.M. van der Kraan, A. Zwijnenburg, M. Makkee, J.A. Moulijn, L. de Jongh, Catal. Today 72 (2002) 95.
[26] G.A. Parks, Chem. Rev. 65 (1965) 177.
[27] M. Haruta, S. Tsubota, T. Kobayashi, H. Kageyama, M.J. Genet, B. Delmon, J. Catal. 144 (1993) 175.
[28] B. Schumacher, Y. Denkwitz, V. Plzak, M. Kinne, R.J. Behm, J. Catal. 224 (2004) 449.
[29] K.H. Choi, B.Y. Coh, H.I. Lee, Catal. Today 44 (1998) 205.
[30] Y. Iizuka, H. Fujiki, N. Yamauchi, T. Chijiiwa, S. Arai, S. Tsubota, M. Haruta, Catal. Today 36 (1997) 115.
[31] M.M. Schubert, M.J. Kahlich, H.A. Gasteiger, R.J. Behm, J. Power Sources 84 (1999) 175.
[32] T. Fukushima, S. Galvagno, G. Parravano, J. Catal. 57 (1979) 177.
[33] C. Winkler, A.J. Carew, S. Haq, R. Raval, Langmuir 19 (2003) 717.
[34] S.H. Ali, J.G. Goodwin, J. Catal. 171 (1997) 339.
[35] G.S. Hsiao, W. Erley, H. Ibach, Surf. Sci. 405 (1998) L465.
[36] M. Valden, X. Lai, D.W. Goodman, Science 281 (1998) 1647.
[37] M.S. Chen, D.W. Goodman, Science 306 (2004) 252.
[38] N. Lopez, J.K. Norskov, T.V.W. Janssens, A. Carlsson, A. Puig-Molina, B.S. Clausen, J.D. Grunwaldt, J. Catal. 225 (2004) 86.